Revision 1

Paratobermorite, $Ca_4(Al_{0.5}Si_{0.5})_2Si_4O_{16}(OH)\cdot 2H_2O\cdot(Ca\cdot 3H_2O)$, a new tobermorite-supergroup mineral with a novel topological type of the microporous crystal structure

Igor V. Pekov[1], Natalia V. Zubkova[1]*, Nikita V. Chukanov[2], Stefano Merlino[3], Vasiliy O. Yapaskurt[1], Dmitry I. Belakovskiy[4], Alexander B. Loskutov[5], Elena A. Novgorodova[6], Svetlana A. Vozchikova[2], Sergey N. Britvin[7] and Dmitry Yu. Pushcharovsky[1]

[1]Faculty of Geology, Moscow State University, Vorobievy Gory, 119991 Moscow, Russia

[2]Institute of Problems of Chemical Physics, Russian Academy of Sciences, 142432 Chernogolovka, Moscow region, Russia

[3] Accademia Nazionale dei Lincei, Via della Lungara 10, Roma, Italy

[4]Fersman Mineralogical Museum of the Russian Academy of Sciences, Leninsky Prospekt 18-2, 119071 Moscow, Russia

[5]Voykova str., 62-500, 624266, Asbest, Sverdlovsk Oblast, Russia

[6]Voykova str., 67-6, 624266, Asbest, Sverdlovsk Oblast, Russia

[7]St. Petersburg State University, University Emb. 7/9, 199034 St. Petersburg, Russia

*Corresponding author: n.v.zubkova@gmail.com

ABSTRACT

A new mineral paratobermorite with the ideal crystal-chemical formula $Ca_4(Al_{0.5}Si_{0.5})_2Si_4O_{16}(OH)\cdot 2H_2O\cdot(Ca\cdot 3H_2O)$ is a member of the tobermorite group within the tobermorite supergroup. It was found at the Bazhenovskoe chrysotile asbestos deposit, Central Urals, Russia, in cavities of grossular rodingite in association with prehnite, pectolite, thomsonite-Ca, and calcite. Paratobermorite occurs as well-shaped prismatic to acicular crystals up to 1 × 1.5 × 8 mm^3 typically assembled in spray- or bush-like radial clusters or open-work aggregates up to 1.5 cm across which form interrupted crusts up to 3 × 5 cm^2. Paratobermorite is transparent, colorless, pale yellowish, pale beige or pinkish, with vitreous lustre. The mineral is brittle, with the (001) perfect cleavage. The Mohs hardness is *ca*. 3½. $D_{meas.}$ = 2.51 (2) and $D_{calc.}$ = 2.533 g cm^{-3}. Paratobermorite is optically biaxial (+), α = 1.565 (2), β = 1.566 (2), γ = 1.578 (2), $2V_{meas.}$ = 25 (10)º and $2V_{calc.}$ = 32º (589 nm). Optical orientation is: $X = c$, $Y = b$, $Z = a$. The chemical composition of paratobermorite (electron microprobe, H_2O by selective sorption from gaseous products of heating) is: Na_2O 0.40, K_2O 0.28, CaO 36.60, MnO 0.04, BaO 0.07, Al_2O_3 6.46, SiO_2 42.32, H_2O 14.10, total 100.27 wt.%. The empirical formula calculated on the basis of 22 O atoms per formula unit and $(O,OH)_{17}\cdot 5H_2O$ is $Na_{0.09}K_{0.04}Ca_{4.72}Al_{0.92}Si_{5.09}O_{15.69}(OH)_{1.31}\cdot 5H_2O$. As all the other members of the tobermorite supergroup, paratobermorite displays OD character, with two MDO (maximum degree of order) structures, one (MDO1), with non-standard space group F2/d11 and the second (MDO2), just corresponding to the structure-type of the new mineral, with non-standard space group $C112_1/m$; its unit-cell parameters obtained from single-crystal X-ray diffraction data are: a = 11.2220 (4), b = 7.3777 (2), c = 22.9425 (8) Å, γ = 89.990 (3)º, V = 1899.46 (10) $Å^3$, and Z = 4; polytype 2*M*. The crystal structure of paratobermorite is solved on single crystal, R = 8.36%. Like structures of other 'tobermorites 11 Å', it is based on the complex layer built of sheet of seven-fold Ca-centred polyhedra with wollastonite-type chains of *T* tetrahedra attached to Ca-sheet from both

47 sides. The tetrahedral (*T*) sites *T*1 and *T*2 are fully occupied by Si while alternating *T*3 and *T*4 sites
48 are filled by Al and Si in the ratio 1:1. The chains of tetrahedra belonging to neighboring complex
49 layers share common oxygen vertices of the bridging *T*3,4 tetrahedra to form xonotlite-type ribbons
50 $[Si_6O_{17}]^{\infty}$. The heteropolyhedral Ca-*T*-O scaffolding appears as a microporous quasi-framework with
51 wide channels which contain additional Ca atoms and H_2O molecules. The complex Ca-*T*-O layers
52 in paratobermorite (so-called *complex modules of type A*) significantly differ in topology (mutual
53 arrangement of *T* tetrahedra and Ca polyhedra) from the complex Ca-*T*-O layers in tobermorite
54 (*complex modules of type B*). The IR spectrum confirms the presence of nonequivalent H_2O
55 molecules and nonequivalent *T*–O–*T* angles involving *T* atoms of two neighboring wollastonite-type
56 chains. Due to the original topological type of the structure and the presence of significant amount
57 of Al which substitutes Si, paratobermorite can be considered as a novel microporous material, a
58 perspective cation-exchanger.
59
60 **Keywords**: paratobermorite, tobermorite group, new mineral, calcium silicate hydrate, OD
61 character, crystal structure, IR spectroscopy, Portland cement, ion exchanger, rodingite,
62 Bazhenovskoe deposit
63

This is the peer-reviewed, final accepted version for American Mineralogist, published by the Mineralogical Society of America.
The published version is subject to change. Cite as Authors (Year) Title. American Mineralogist, in press.
DOI: https://doi.org/10.2138/am-2022-8284. http://www.minsocam.org/

INTRODUCTION

Tobermorite-supergroup members (or 'tobermorites') belong to a large family of calcium silicate hydrate (C-S-H) compounds, which includes many natural and synthetic representatives. For many years, 'tobermorites' have been in the focus of research by crystal chemists and material scientists due to their close relationships with the C-S-H compounds formed during the Portland cement hydration (Richardson 2008). In addition, 'tobermorites' demonstrate cation exchange properties and can be used in waste disposal (Bonaccorsi and Merlino 2005). Natural 'tobermorites' are united in the tobermorite supergroup. Until recently, this supergroup included five mineral species: tobermorite, kenotobermorite (forming the tobermorite group), clinotobermorite, plombiérite, and riversideite (Biagioni et al. 2015; see below for details).

In this paper we describe a new representative of the tobermorite group which differs from other members of the tobermorite supergroup not only in chemical features, symmetry and unit-cell metrics but also in the topology of the crystal structure, which is the most significant individual feature of the new mineral. It is named **paratobermorite** from the Greek παρα for "near" and the relationship to tobermorite. Both the new mineral and its name have been approved by the Commission on New Minerals, Nomenclature and Classification of the International Mineralogical Association (IMA No. 2020–100). The type specimen is deposited in the systematic collection of the Fersman Mineralogical Museum of the Russian Academy of Sciences, Moscow under the catalogue number 97513.

TOBERMORITE-SUPERGROUP MINERALS:

HISTORICAL BACKGROUND AND GENERAL CRYSTAL CHEMICAL FEATURES

Historically, among 'tobermorites' three types of minerals, so-called tobermorites 14 Å, 11 Å, and 9 Å were distinguished in correspondence with the strongest basal *d*-spacing in a powder X-ray diffractogram. In terms of mineral names, they correspond to plombiérite, tobermorite, and riversideite, respectively (Taylor 1953, 1964; McConnell 1954). The name tobermorite was introduced in the mineralogy by Heddle (1880), for a new mineral described from four localities in Scotland, including three near Tobermory. Claringbull and Hey (1952), who re-examined the Heddle's material, found that tobermorite is an individual natural C-S-H phase, which demonstrates the main basal reflection of powder X-ray diffraction (XRD) pattern with d = 11.3 Å. Based on this, McConnell (1954) applied the mineral name tobermorite to the C-S-H compounds with a 11 Å main basal spacing.

The structure model for tobermorite (tobermorite *s.s.*, or 'tobermorite 11 Å') was firstly suggested by Megaw and Kelsey (1956) and later elaborated by Mamedov and Belov (1958) and Hamid (1981). The real structure of 'tobermorite 11 Å', its structural variations and polytypism were studied by Merlino et al. (1999, 2001) and Merlino and Bonaccorsi (2008). Hydrogen-bearing groups in one of varieties of 'tobermorite 11 Å' were examined in detail by Churakov (2009). Clinotobermorite, a natural C-S-H phase with a 11 Å main basal *d*-spacing, dimorphous with tobermorite, was described as a new mineral species from Fuka, Okayama Prefecture, Japan (Henmi and Kusachi, 1992). Its sub-cell structure was determined by Hoffmann and Armbruster (1997), whereas the real structure was defined by Merlino et al. (2000).

In 2015, the IMA-approved nomenclature of the tobermorite supergroup was published. In the frame of this nomenclature (Biagioni et al. 2015), five valid mineral species were distinguished and clearly defined. 'Tobermorites 14 Å' are represented by plombiérite with the idealized, end-member formula $Ca_5Si_6O_{16}(OH)_2 \cdot 7H_2O$, 'tobermorites 9 Å' by riversideite with the end-member formula $Ca_5Si_6O_{16}(OH)_2$ and 'tobermorites 11 Å' include three species. Tobermorite and

clinotobermorite are defined as dimorphs with the idealized, end-member formula $Ca_5Si_6O_{17}\cdot 5H_2O$. Besides this pair, 'tobermorites 11 Å' include kenotobermorite with the end-member formula $Ca_4Si_6O_{15}(OH)_2\cdot 5H_2O$ (Table 1).

The fundamental building unit in the crystal structure of all tobermorite-supergroup minerals is the complex module (or complex layer) consisting of a sheet of seven-coordinated Ca-centred polyhedra decorated from both sides by Si-centred tetrahedra (*T*) belonging to wollastonite-type chains $[Si_3O_9]^{\infty}$ (Merlino and Bonaccorsi 2008). This complex module is *C*-centred and has the periods $a \approx 11.2$ Å, $b \approx 7.3$ Å and thickness $c_0 \approx 11.2$ Å (Merlino et al. 1999, 2000, 2001; Biagioni et al. 2015). In Fig. 1, the complex module is illustrated by the examples taken from 'tobermorites 11 Å'. As distinct from plombiérite, in 'tobermorites 11 Å' the stacking of the complex modules gives rise to the condensation of wollastonite-type chains of tetrahedra to form the $[Si_6O_{17}]^{\infty}$ double chains (Merlino and Bonaccorsi 2008), also known as xonotlite-type ribbons. In cavities (channels) within the resulting heteropolyhedral Ca-*T*-O quasi-framework, additional cations (typically, Ca, up to one atom per formula unit, below *apfu*) and H_2O molecules occur (Fig. 2). In particular, the presence or absence of Ca in these cavities is a cause of the difference in the number of Ca *apfu* between tobermorite $Ca_5Si_6O_{17}\cdot 5H_2O$ and kenotobermorite $Ca_4Si_6O_{15}(OH)_2\cdot 5H_2O$ (Biagioni et al. 2015). The presence of these wide channels confers the properties of 'tobermorites' as ion-exchangers.

Bonaccorsi and Merlino (2005) stressed that there are two geometrically distinct ways to place the chains of tetrahedra on the two sides of the calcium sheet in the complex module. In the first one, the bridging tetrahedra are placed at right on one side and at left on the other side (or vice versa), with respect to the disilicate groups of the corresponding chain. Such layer was marked as *complex module of type A*. In the second way, the bridging tetrahedra on both sides are all placed at left (or all placed at right) with respect to the corresponding disilicate groups. The layer of this type was called *complex module of type B* (Bonaccorsi and Merlino 2005; Biagioni et al. 2015). Thus, the

This is the peer-reviewed, final accepted version for American Mineralogist, published by the Mineralogical Society of America.
The published version is subject to change. Cite as Authors (Year) Title. American Mineralogist, in press.
DOI: https://doi.org/10.2138/am-2022-8284. http://www.minsocam.org/

complex modules of types A and B are topologically different (Fig. 1). The complex module of type B is known in tobermorite and kenotobermorite, whereas the complex module of type A is known in clinotobermorite. Now it is found in paratobermorite.

POLYTYPIC ASPECTS IN TOBERMORITE GROUP OF MINERALS

The various members of the 'tobermorite supergroup' present an order-disorder (OD) character (Dornberger-Schiff 1956, 1964, 1966; Ferraris et al. 2008) related to the metrical relationships between the calcium polyhedral module, with a repeat of 3.56 Å, and the wollastonite-type chains, with a periodicity of 7.3 Å. The chains may be connected to the calcium layers in two distinct but equivalent positions, shifted by 3.65 Å in the **b** direction. Consequently, the various phases of the tobermorite supergroup can be described in terms of OD layers which may stack in two different ways along **c***, giving rise to a whole family of disordered or ordered sequences (polytypes).

In all the polytypes of a family (but also in the disordered sequences) pairs of adjacent layers are geometrically equivalent (principle of OD structures). In each family two main polytypes exist, corresponding to the sequences in which not only pairs but also triples, quadruples,… *n*-tuples of layers are geometrically equivalent, corresponding to the MDO (Maximum Degree of Order) structures.

In the case of tobermorite (tobermorite 11Å), kenotobermorite and paratobermorite the OD layer (Fig. 3) presents layer symmetry *C*2*m*(*m*) (one of the possible eighty layer groups), with translation vectors **a** and **b**, third vector $\mathbf{c_0}$ ($a \sim 11.3$, $b \sim 7.35$, $c_0 \sim 11.2$ Å). The parentheses in the last position of the symbol for the layer group indicate the direction of missing periodicity.

For a layer with symmetry *C*2*m*(*m*) there are two possible sets of σ-operations (operations which relate adjacent layers) compatible with the set of λ-operations (Ferraris et al. 2008)

This is the peer-reviewed, final accepted version for American Mineralogist, published by the Mineralogical Society of America.
The published version is subject to change. Cite as Authors (Year) Title. American Mineralogist, in press.
DOI: https://doi.org/10.2138/am-2022-8284. http://www.minsocam.org/

$$\begin{matrix} C & 2 & m & (m) \\ \{\ 2_s & n_{2,s} & (n_{s,r})\ \} \end{matrix} \qquad \begin{matrix} C & 2 & m & (m) \\ \{\ n_{r,2} & 2_r & (2_2)\ \} \end{matrix} \qquad (1)$$

The first of them, with value ½ for both *s* and *r* parameters, results in the OD groupoid family symbol

$$\begin{matrix} C & 2 & m & (m) \\ \{\ 2_{1/2} & n_{2,1/2} & (n_{1/2,1/2})\ \} \end{matrix}$$

which just consents the derivation of the real structure of tobermorite and kenotobermorite and the definition of their two main polytypes (MDO structures) (Merlino et al. 1999; 2001; Biagioni et al. 2015).

It seems proper to recall that the symbols used for the σ-operations are in keeping with those used in the normal space group operations: $2_{1/2}$ represents a rotation of 180° followed by translation along **a** of *a*/4; $n_{2,1/2}$ represents a glide normal to **b** with translational components $\mathbf{c_0}$ and **a**/4; $n_{1/2,1/2}$ represents a glide normal to $\mathbf{c_0}$, with translational components **a**/4 and **b**/4.

Layers of *C*2*mm* symmetry follow each other in the **c** direction, related by the operator $n_{1/2,1/2}$ (= $n_{-1/2,-1/2}$ due to the *C* centring of the single layer) normal to **c**, or by the operator $n_{1/2,-1/2}$ (= $n_{-1/2,1/2}$).

The polytype MDO1 corresponds to the sequence in which the operators $n_{1/2,1/2}$ and $n_{1/2,-1/2}$ regularly alternate, resulting in a structure with *F*2*dd* symmetry and cell parameters *a* ~ 11.3, *b* ~ 7.35, *c* ~ 45.2 Å (Merlino et al., 2001). MDO2 corresponds to the sequence in which the operator $n_{1/2,1/2}$ is constantly applied, resulting in a structure with *C* centred cell, with parameters *a* ~ 11.3, *b* ~ 7.35, *c* ~ 22.6 Å, γ ~ 90°, presenting additional lattice points at ¼, ¼, ½ and ¾, ¾, ½ (Fig. 3 in Merlino et al., 2001). A convenient cell may be derived through the transformations **a**' = (**a** + **b**)/2, **b**' = **b**, **c**' = c , thus obtaining a *B* centred monoclinic cell, space group *B*11*m* and cell parameters *a* ~ 6.73, *b* ~ 7.35, *c* ~ 22.6 Å, γ ~ 122.9°.

This is the peer-reviewed, final accepted version for American Mineralogist, published by the Mineralogical Society of America.
The published version is subject to change. Cite as Authors (Year) Title. American Mineralogist, in press.
DOI: https://doi.org/10.2138/am-2022-8284. http://www.minsocam.org/

In a paper by Merlino and Bonaccorsi (2008), attention has been given to the second set of σ-operations compatible with the layer group symmetry *C*2*m*(*m*). By assuming the value ½ for the *r* parameter a new OD groupoid family was obtained which has the symbol

$$C \quad 2 \quad m \quad (m)$$
$$\{\, n_{1/2,2} \quad 2_{1/2} \quad (2_2) \,\}$$

and by which a new family of OD structures may be obtained.

Merlino and Bonaccorsi (2008) indicated that also in the present case two main polytypes exist: MDO1 is obtained through the constant application of the [$n_{1/2,2}$ - -] operation and presents non-standard space group *F*2/*d*11, with *a* = 11.3, *b* = 7.35, *c* = 45.2 Å, α = 90°; MDO2 is obtained through the regular alternation of the operations [$n_{1/2,2}$ - -] and [$n_{-1/2,2}$ - -] and presents non-standard space group $C112_1/m$, with *a* = 11.3, *b* = 7.35, *c* = 22.6 Å, γ = 90°. The unit cell dimensions, space group and structural arrangement of the last polytype closely correspond to those of paratobermorite, the mineral species described in the present paper.

Tobermorite and kenotobermorite share the same OD family, but show distinguished chemical composition, $Ca_5Si_6O_{17}\cdot 5H_2O$ for tobermorite and $Ca_4Si_6O_{15}(OH)_2\cdot 5H_2O$ for kenotobermorite. As regards the polytypic aspects both main polytypes of kenotobermorite have been observed in nature: kenotobermorite-2*M* (*B*11*m*, *a* = 6.735, *b* = 7.385, *c* = 22.487 Å, γ = 123.25°) and kenotobermorite-4*O* (*F*2*dd*, *a* = 11.265, *b* = 7.385, *c* = 44.97 Å), respectively; whereas only the monoclinic polytype tobermorite-2*M* (*B*11*m*, *a* = 6.732, *b* = 7.369, *c* = 22.680 Å, γ = 123.18°) has been found. Paratobermorite, $Ca_5AlSi_5O_{16}(OH)\cdot 5H_2O$ has a peculiar OD character, pertaining to a different OD family. Similar to the case of tobermorite, so far only the polytype paratobermorite-2*M* has been found in nature.

ANALYTICAL METHODS AND DATA PROCESSING DETAILS

This is the peer-reviewed, final accepted version for American Mineralogist, published by the Mineralogical Society of America.
The published version is subject to change. Cite as Authors (Year) Title. American Mineralogist, in press.
DOI: https://doi.org/10.2138/am-2022-8284. http://www.minsocam.org/

The chemical composition of paratobermorite was determined by electron microprobe in the Laboratory of Analytical Techniques of High Spatial Resolution, Dept. of Petrology, Moscow State University (MSU) using a Jeol JSM-6480LV scanning electron microscope (SEM) equipped with an INCA-Wave 500 wavelength-dispersive spectrometer, with an acceleration voltage of 20 kV, a beam current of 10 nA; the electron beam was rastered to the 5×5 μm^2 area. The standards used are listed in Table 2. The studies of morphology of paratobermorite crystals and aggregates, including the obtaining of SEM images, were carried out using the same scanning electron microscope.

H_2O was determined by the Alimarin method [the Penfield method modified for small samples and involving selective sorption of H_2O on $Mg(ClO_4)_2$ from gaseous products obtained by heating the mineral at 1080°C in oxygen at 1 atm]. Two measurements were performed and the results were averaged. The attempt to measure CO_2 content was made using the method of selective sorption of CO_2 on askarite (an asbestiform material saturated with NaOH) from gaseous products obtained by heating the mineral at 1080°C in oxygen at 1 atm. This experiment showed the absence of CO_2 in paratobermorite (that is in agreement with both IR spectroscopy and structure data: see below).

In order to obtain infrared (IR) absorption spectrum, powdered sample of paratobermorite was mixed with anhydrous KBr, pelletized, and analyzed using an ALPHA FTIR spectrometer (Bruker Optics) at a resolution of 4 cm^{-1}. A total of 16 scans were collected. The IR spectrum of an analogous pellet of pure KBr was used as a reference. A sample of tobermorite (tobermorite-2*M*) from the Pervomaiskiy quarry, Mt. Bol'shoy Kermen, Bakhchisaray district, Crimea Peninsula was prepared and studied using the same procedures for comparison.

Powder XRD study of paratobermorite was carried out using a Rigaku R-AXIS Rapid II single-crystal diffractometer equipped with a curved image plate detector (Debye-Scherrer geometry, r = 127.4 mm) and Co$K\alpha$ radiation source (rotating anode; 40 kV, 15 mA, and 12 min

exposure time; powdered sample of spherical form prepared with X-ray amorphous glue was studied), with Rigaku VariMax microfocus mirror optics. Imaging plate-to-profile data conversion was performed using osc2xrd software (Britvin et al. 2017).

Single-crystal XRD studies of paratobermorite were carried out on a crystal of 0.21 × 0.30 × 0.63 mm^3 in size using an Xcalibur S single-crystal diffractometer equipped with a CCD detector. A full sphere of three-dimensional data was collected. Data reduction was performed using CrysAlisPro version 1.171.39.46 (Rigaku OD 2018). The data were corrected for Lorentz factor and polarization effect.

The crystal structure of paratobermorite was solved by direct methods and refined using the SHELX software package (Sheldrick 2015) to $R = 0.0831$ for 2076 unique reflections with $I > 2\sigma(I)$ in the frame of monoclinic space group $P2_1/m$ [unit-cell parameters: $a = 6.7149(2)$, $b = 22.9441(8)$, $c = 6.7162(3)$ Å, $\beta = 113.358(4)°$]. In this setting, the a and c parameters of the unit cell have nearly the same values, and the transition to a pseudo-orthorhombic unit cell can be performed by applying the matrix 1 0 -1 / 1 0 1 / 0 -1 0. The unit cell obtained in that way is comparable with those suggested for tobermorite ('tobermorite 11 Å') and other closely related tobermorite-supergroup minerals reported in recent papers (Merlino et al. 1999, 2000, 2001; Merlino and Bonaccorsi 2008; Biagioni et al. 2015): see Table 1. We have re-integrated single-crystal XRD data and refined the structure model of paratobermorite in the non-standard space group $C112_1/m$ to $R = 0.0836$ for 2055 unique reflections with $I > 2\sigma(I)$. For an easier comparison, $C112_1/m$ is chosen by us as the "natural" space group for paratobermorite, consenting an easy comparison with the other ‘tobermorite 11 Å’ phases (Table 1). In both structure models of paratobermorite, microtwinning was observed. The transition matrices 0 0 1 / 0 -1 0 / 1 0 0 (sp. gr. $P2_1/m$) and -1 0 0 / 0 1 0 / 0 0 1 (sp. gr. $C112_1/m$) are found, and the refined twin ratio is 0.53 : 0.47. Complete sets of crystallographic data for both

models, with the space groups $P2_1/m$ and $C112_1/m$, can be retrieved from the CIF files attached as the Supplementary Material.

All attempts to obtain a reasonable structure model for paratobermorite in the frame of orthorhombic symmetry unit cell were unsuccessful. The *PLATON* program (Spek 2003) did not detect higher metrics or crystallographic symmetry for the monoclinic model.

RESULTS AND DISCUSSION

Occurrence

Paratobermorite was found at the Bazhenovskoe deposit of chrysotile asbestos located at the eastern border of the city of Asbest, Sverdlovsk Oblast, Central (Middle) Urals, Russia.

The Bazhenovskoe deposit related to the Bazhenovsky gabbro-harzburgite intrusion is one of the world-largest deposits of high-quality chrysotile asbestos. It was discovered in 1885 and is operated since 1889. From the mineralogical viewpoint, Bazhenovskoe is mainly known due to rodingites formed as a result of a low-grade metamorphism after numerous gabbro dikes hosted by serpentinites. Geological and mineralogical data on Bazhenovskoe rodingites were summarized by Erokhin (2017).

One of the bright mineralogical features of the Bazhenovskoe deposit is the abundance and diversity of C-S-H minerals in late, hydrothermal parageneses related to rodingites. Some of them are known here in the form of large and perfect crystals, which is unusual for these minerals. The studies of samples from Bazhenovskoe gave a significant contribution to the mineralogy and crystal chemistry of calcium silicate hydrates, namely tobermorite, plombiérite (Zadov et al. 1995, 2001; Merlino et al. 2001), rosenhahnite (Zadov et al. 2000), and oyelite (Pekov et al. 2019). The discovery of paratobermorite again highlights the important role of the Bazhenovskoe deposit for the mineralogy of calcium silicate hydrates.

This is the peer-reviewed, final accepted version for American Mineralogist, published by the Mineralogical Society of America.
The published version is subject to change. Cite as Authors (Year) Title. American Mineralogist, in press.
DOI: https://doi.org/10.2138/am-2022-8284. http://www.minsocam.org/

The specimens with the new mineral were collected in 2019 from a rodingite vein uncovered in the eastern part of the Southern open pit operating on the Bazhenovskoe deposit. This steeply dipping (with the dipping angle of 70–80º) vein about 0.5 m thick is seated in serpentinites and has a near-meridional orientation. In the area where paratobermorite was found, the main rodingite-forming mineral is white, colorless or grayish massive, fine-grained grossular and the subordinate mineral is prehnite. Paratobermorite occurs in cavities together with pectolite (represented by both 1*A* and *M*2*abc* polytypes), thomsonite-Ca, and calcite. Paratobermorite is a hydrothermal mineral crystallized in a Ca-rich assemblage related to rodingite, a rock formed as a result of metasomatic alteration (rodingitization) of a gabbroid dyke cross-cutting serpentinite (Erokhin 2017 and references therein).

General appearance, crystal morphology, physical properties and optical data

Paratobermorite forms prismatic to acicular crystals, elongated along [010], up to 1 mm × 1.5 mm × 8 mm. They are well-shaped, perfectly terminated (Figs. 4 and 5a,b) or crude (Fig. 5c), sometimes divergent, and typically assembled in open-work aggregates (Figs. 5c and 6a) up to 1 cm × 1.5 cm, spray- or bush-like radial clusters (Fig. 6b) up to 1.3 cm across. Crystal crusts, usually interrupted, of paratobermorite up to 3 cm × 5 cm in area and up to 1 cm thick cover grossular and prehnite aggregates whereas pectolite, thomsonite-Ca and calcite overgrow paratobermorite.

Noteworthy, unlike other 'tobermorites', which typically occur (in particular, at Bazhenovskoe) as thin acicular to hair-like individuals (tobermorite, clinotobermorite) or scales (plombiérite), paratobermorite forms relatively thick prismatic crystals (Figs. 4–6). The prismatic zone of paratobermorite crystals is formed by the {100} and {001} faces and the terminations are formed by the {011} faces (Fig. 4: the pseudo-orthorhombic setting with $\gamma = 90^{\circ}$ is used). Contact twins on {100} were observed under the microscope in polarized transmitted light; microtwinning

306 with the same plane (100) as a twinning operator (the matrix is -1 0 0 / 0 1 0 / 0 0 1) was found
307 during the crystal structure determination.

308 Paratobermorite is transparent, colorless, pale yellowish, pale beige or pinkish, with white
309 streak and vitreous lustre. The mineral does not fluoresce in ultraviolet light. Paratobermorite is
310 brittle, the (001) perfect cleavage is observed, and the fracture is stepped. The Mohs hardness is *ca*.
311 3½. Density measured by flotation in heavy liquids (bromoform + heptane) is equal to 2.51 (2) g
312 cm^{-3}. Density calculated using the empirical formula and unit-cell volume determined from the
313 single-crystal XRD data is 2.533 g cm^{-3}.

314 Under the microscope, in plane polarized transmitted light paratobermorite is colorless and
315 non-pleochroic. It is optically biaxial (+), α = 1.565 (2), β = 1.566 (2), γ = 1.578 (2), $2V_{meas.}$ = 25
316 (10)º and $2V_{calc.}$ = 32º (589 nm). Dispersion of optical axes was not observed. Extinction is parallel
317 and elongation is negative. Orientation is as follows: $X = c$, $Y = b$, $Z = a$.

318

319 **Chemical composition**

320 The chemical composition of paratobermorite in wt.% is given in Table 2. The charge-
321 balanced empirical formula calculated on the basis of 22 O atoms per formula unit (*apfu*) and
322 $(O,OH)_{17}\cdot 5H_2O$ *pfu* (in accordance with structural data, see below) is
323 $Na_{0.09}K_{0.04}Ca_{4.72}Al_{0.92}Si_{5.09}O_{15.69}(OH)_{1.31}\cdot 5H_2O$. The simplified formula is $Ca_5AlSi_5O_{16}(OH)\cdot 5H_2O$.
324 The ideal crystal-chemical formula of paratobermorite written in accordance with the scheme
325 proposed in the frame of the IMA-accepted nomenclature of tobermorite-supergroup minerals
326 (Biagioni et al. 2015) is $Ca_4(Al_{0.5}Si_{0.5})_2Si_4O_{16}(OH)\cdot 2H_2O\cdot(Ca\cdot 3H_2O)$ (see structure data below).

327 The compatibility index $1 - (K_p/K_c) = -0.008$ if $D_{meas.}$ is used and = 0.001 if $D_{calc.}$ is used.
328 Both values are rated as *superior*, according to Mandarino (1981).

329

330 **Infrared spectroscopy**

331

332 In the IR spectra of paratobermorite and tobermorite (Fig. 7), absorption bands are observed in
333 the ranges of 3200–3600 cm^{-1} (O–H stretching vibrations, 1620–1650 cm^{-1} (H–O–H bending
334 vibrations of H_2O molecules), 920–1220 cm^{-1} (Si–O stretching vibrations), 870–910 cm^{-1} (stretching
335 vibrations involving Al–O bonds), 650–770 cm^{-1} (Ca···O–H and/or O–*T*–O bending vibrations) and
336 below 600 cm^{-1} (lattice modes involving Si–O stretching, Si–O–Si bending and H_2O librational
337 vibrations). For the assignment of the IR bands see (Zadov et al. 2001, 2006; Organova et al. 2002;
338 Chukanov and Chervonnyi 2016).
339 The main differences between the IR spectra of tobermorite and paratobermorite are observed in the
340 ranges of 650–770, 870–910, 1100–1220, and 3200–3600 cm^{-1} which may be due to significant
341 differences between these minerals in the Al:Si ratio, stacking of wollastonite-type chains, and
342 hydrogen bonding. In particular, the strong IR band at 878 cm^{-1} is a specific feature of paratobermorite.
343 This band is not observed in IR spectra of Al-poor tobermorite-group minerals. As it was shown
344 earlier (Chukanov 2014), in silicates with polymerized SiO_4 tetrahedra, the position of the most
345 high-frequency Si–O-stretching band, $\nu_{Si-O}(max)$, observed in the range of 1000–1220 cm^{-1},
346 depends on the value of the greatest Si–O–Si angle, φ_{SiOSi}. At $\varphi_{SiOSi} = 180°$ the value $\nu_{Si-O}(max)$ is
347 close to 1200 cm^{-1}. For example, in the IR spectrum of xonotlite (with $\varphi_{SiOSi} = 180°$ at the stacking
348 of wollastonite-type chains: see Kudoh and Takeuchi 1979) $\nu_{Si-O}(max)$ is equal to 1203 cm^{-1}. The
349 crystal structure of tobermorite is also based on xonotlite-like ribbons with the φ_{SiOSi} angle close to
350 180° (Merlino et al. 2001). For Al-free tobermorite the $\nu_{Si-O}(max)$ value is in the range of 1200–
351 1215 cm^{-1}. In the IR spectra of minerals belonging to the palygorskite and the sepiolite groups and
352 structurally related minerals ("palysepioles", with $\varphi_{SiOSi} \approx 180°$ at the stacking of bands of
353 tetrahedra: Cámara et al. 2002; Ferraris and Gula 2005; Chukanov et al. 2012) $\nu_{Si-O}(max)$ varies

354 from 1160 to 1212 cm^{-1}. Another example is suolunite $Ca_2[Si_2O_5(OH)_2]\cdot H_2O$ (Ma et al. 1999) with
355 φ_{SiOSi} = 180°, ν_{Si-O}(max) = 1191 cm^{-1}. In contrast to these examples, for cuspidine $Ca_8(Si_2O_7)_2F_4$
356 (Saburi et al. 1977) φ_{SiOSi} = 155.4°, ν_{Si-O}(max) = 1057 cm^{-1}; for kilchoanite $Ca_6(Si_3O_{10})(SiO_4)$
357 (Taylor 1971) φ_{SiOSi} = 117°, ν_{Si-O}(max) = 1047 cm^{-1}.

358 The presence of the bands at 1120 and 1167 cm^{-1} in the IR spectrum of paratobermorite
359 (unlike tobermorite: Fig. 7b) indicates the presence of two kinds of the Si–O–Si bridges with large
360 (but significantly smaller than 180°) Si–O–Si angles and is in good agreement with the values of the
361 *T*4–O*T*4–*T*4 and *T*3–O*T*3–*T*3 angles [161(2)° and 174.0(12)°, respectively]. Unlike, the IR spectra
362 of tobermorite contain a single band in the range of 1160–1220 cm^{-1} (typically, 1200 ± 20 cm^{-1}:
363 Chukanov 2014) which corresponds to a Si–O–Si angle close to 180°.

364 As compared to tobermorite, paratobermorite is characterized by lower wavenumbers of the
365 bands corresponding to O–H stretching vibrations and, consequently, by stronger hydrogen bonds.
366 Based on the correlation reported by Libowitzky (1999), the D···A distances for hydrogen bonds in
367 paratobermorite corresponding to the bands at 3220, 2446, and 3538 cm^{-1} are equal to 2.71, 2.83, and
368 2.97 Å, respectively. Bands of carbonate and orthoborate anions are not observed in the IR spectrum
369 of paratobermorite.

370

371 **X-ray diffraction data and crystal structure**

372 Powder XRD data of paratobermorite are given in Table 3. Parameters of the monoclinic unit
373 cell calculated from powder data are: *a* = 11.245 (3), *b* = 7.391 (2), *c* = 23.01 (1) Å, γ = 90.00 (5)º
374 and *V* = 1912 (2) $Å^3$.

375 The unit-cell parameters obtained for paratobermorite from single-crystal XRD data are: *a* =
376 11.2220 (4), *b* = 7.3777 (2), *c* = 22.9425 (8) Å, γ = 89.990 (3)º, and *V* = 1899.46 (10) $Å^3$.

377 The crystal structure description of paratobermorite is reported here for the model in the
378 space group $C112_1/m$. Selected interatomic distances are given in Table 4 and bond valence
379 calculations in Table 5.

380 The crystal structure of paratobermorite (Fig. 2), like structures of other 'tobermorites 11 Å'
381 (Merlino et al. 2001), is based on the complex module built of sheet of Ca-centred polyhedra,
382 parallel to (001), with chains of *T* tetrahedra running along the *b* axis and attached to Ca-sheet.
383 Paratobermorite possesses the *complex module of type A* (Fig. 1a). There are three main *T* sites;
384 according to interatomic distances, *T*1 and *T*2 are fully occupied by Si atoms while the *T*3 site, as
385 well as the additional *T*4 site (these sites could be only alternatively occupied due to a short *T*3–*T*4
386 distance) are filled by Al and Si in the ratio 1:1; the site occupancy factors of *T*3 and *T*4 are 0.70 and
387 0.30, respectively. The chains of tetrahedra belonging to neighboring complex modules share
388 common oxygen vertices of the bridging *T*3,4 tetrahedra to form double chains (xonotlite-type
389 ribbons); in general, the heteropolyhedral Ca-*T*-O scaffolding appears as a microporous quasi-
390 framework. Two main Ca sites (Ca1 and Ca2) occupy seven-fold polyhedra which build the (001)
391 layers of the complex module. Wide channels in the quasi-framework contain two sites partially
392 occupied with Ca (additional Ca sites labelled as Ca3 and Ca4 in Tables 4 and 5 and Fig. 2) and five
393 partially occupied H_2O sites. Water molecules (labelled as Ow1–Ow5 in Tables 4 and 5) are placed
394 on the *m* plane and for better clarity their further site splitting and positional disorder were forbidden
395 during the refinement. In terms of polytypism (Merlino and Bonaccorsi 2008; Biagioni et al. 2015),
396 paratobermorite is represented by the 2*M* polytype.
397

398 **Comparison of paratobermorite with other tobermorite-supergroup minerals**

399 Paratobermorite belongs to 'tobermorites 11 Å', as well as tobermorite, kenotobermorite and
400 clinotobermorite. All known polytypes of these minerals are reported in Table 1.

This is the peer-reviewed, final accepted version for American Mineralogist, published by the Mineralogical Society of America.
The published version is subject to change. Cite as Authors (Year) Title. American Mineralogist, in press.
DOI: https://doi.org/10.2138/am-2022-8284. http://www.minsocam.org/

Based on the structure arrangement, paratobermorite is included in the tobermorite group within the tobermorite supergroup, together with tobermorite and kenotobermorite. The belonging of paratobermorite to the tobermorite group is justified by the same type of tetrahedral motif in the structure (Fig. 8a,b) whereas clinotobermorite (Fig. 8c) and other tobermorite-supergroup members differ from them in this aspect and, thus, do not belong to the tobermorite group (Biagioni et al. 2015).

The peculiar aspects which characterize paratobermorite as an individual mineral species and distinguish it from tobermorite and other related minerals, are as follows.

(1) The essential building units of the crystal structures of paratobermorite and related minerals are topologically different. The complex Ca-*T*-O layer in the structure of paratobermorite is the *complex module of type A* (Fig. 1a) whereas the complex Ca-*T*-O layer in tobermorite is the *complex module of type B* (Fig. 1b). They significantly differ from each other in the mutual arrangement of *T* tetrahedra and Ca polyhedra (see above). From clinotobermorite, paratobermorite significantly differs in the general topological characteristics of the tetrahedral motif (Figs. 8a,c). Tobermorite differs from both these minerals in this aspect (Fig. 8b).

(2) In terms of crystal chemistry, paratobermorite differs from all other tobermorite-supergroup minerals in the Al-Si ordering: it is not the only mineral significantly enriched with Al but it is the first member of the group in which Al-Si ordering is found. The bridging *T*3,4 tetrahedra which connect adjacent complex layers in the whole structure are occupied by Si and Al atoms in the ratio 1:1 whereas the *T*1,2 tetrahedra are occupied by Si (Tables 4 and 5, Figs. 1, 2 and 8). All other structurally studied minerals of the tobermorite-supergroup display Si-Al disorder: in their structures, all *T* tetrahedra are essentially Si-dominant (Merlino et al. 1999, 2000, 2001; Bonaccorsi et al. 2005 and references therein). For this reason, the simplified formula of paratobermorite $Ca_5AlSi_5O_{16}(OH)\cdot 5H_2O = Ca_5(AlSi)Si_4O_{16}(OH)\cdot 5H_2O$, differs from all other valid minerals of the tobermorite supergroup that have the simplified formulae with only Si in the tetrahedral part

(Biagioni et al. 2015; Table 1) and explains the larger value of the *c* parameter in comparison with that of the other members of the tobermorite group.

(3) Paratobermorite differs from all other tobermorite-supergroup minerals in space group and metrics of the unit cell that is a consequence of the above-discussed differences in the topology of structure. The crystal data for 'tobermorites 11 Å' are summarized in Table 1 and the *ac* projections of the chains of tetrahedra in the unit cells of tobermorite-2*M*, paratobermorite-2*M* and clinotobermorite-2*M* (*i.e.*, monoclinic polytypes with $c = 22.5 – 23$ Å) are shown in Fig. 8.

IMPLICATIONS

Due to the original topological type of the crystal structure, paratobermorite can be considered as a novel microporous material known only as a natural compound. Despite the fact that it has not yet been synthesized, the discovery of paratobermorite at the Bazhenovskoe deposit makes possible to study its properties. This finding has both scientific and applied value. On one hand, it confirmed the previously predicted (Merlino and Bonaccorsi 2008) existence of a tobermorite-like structure of this topological type. On the other hand, one can expect the presence of paratobermorite as one of the phases in some cement materials (mainly in Portland cement), especially, materials with a relatively high aluminum content. The upper limit of the substitution of Si for Al in 'tobermorites 11 Å' corresponds to the atomic ratio Al:(Al+Si) of 0.167 which corresponds to the situation Si–O–Al around all O atoms bridging the wollastonite-type chains. In the case of paratobermorite, this ratio is equal to 0.153, which exceeds the maximum Al:(Al+Si) values of 0.13 – 0.14 known for synthetic 'tobermorites' (Sakiyama et al. 2000). The formation of Al-rich tobermorite-related compounds occurs most probably in some kinds of Al-rich cements containing active SiO_2. Concretes and ceramics prepared from such cements show significant growth of strength with time (El-Didamony et al. 2000; Chervonnyi et al. 2010). The ion-exchange capability is mainly exhibited by Al-substituted tobermorite-related compounds (Bonaccorsi and Merlino

2005). In particular, these compounds show sorption capacity for a number of transition metals (Al-Wakeel et al. 2001) and a high selectivity for Cs^+ and Li^+ (Tsuji et al. 1991 and references therein). Thus, paratobermorite can be considered as a perspective prototype of microporous materials with technologically important properties (cation-exchanger), probably better than ordinary, Al-poor tobermorites.

ACKNOWLEDGMENTS

We thank two anonymous referees and Associate Editor Diego Gatta for valuable comments. This work was supported by the Russian Foundation for Basic Research, grant no. 18-29-12007-mk (mineralogical characterization, crystal structure determination and crystal chemical analysis). The IR spectroscopic investigation was carried out in accordance with the state task, state registration number AAAA-A19-119092390076-7. The technical support by the St. Petersburg State University X-Ray Diffraction Resource Center in powder XRD study of paratobermorite is acknowledged.

REFERENCES CITED

Al-Wakeel, E.I., El-Korashi, S.A., El-Hamaly, S.A., and Rizk, M.A. (2001) Divalent ion uptake of heavy metal cations by (aluminium + alkali metals)-substituted synthetic 1.1 nm tobermorites. Journal of Materials Science, 36, 2405–2415.

Biagioni, C., Merlino, S., and Bonaccorsi, E. (2015) The tobermorite supergroup: a new nomenclature. Mineralogical Magazine, 79, 485–495.

Bonaccorsi, E. and Merlino, S. (2005) Modular microporous minerals: cancrinite-davyne group and C-S-H phases. Reviews in Mineralogy and Geochemistry. Micro- and Mesoporous Mineral Phases. Eds: G. Ferraris and S. Merlino, 57, 241–290.

475 Britvin, S.N., Dolivo-Dobrovolsky, D.V., and Krzhizhanovskaya, M.G. (2017) Software for
476 processing the X-ray powder diffraction data obtained from the curved image plate detector of
477 Rigaku RAXIS Rapid II diffractometer. Zapiski Rossiiskogo Mineralogicheskogo
478 Obshchestva, 146(3), 104–107 (in Russian).
479 Cámara, F., Garvie, L.A.J., Devouard, B., Groy, T.L., and Buseck, P.R. (2002) The structure of Mn-
480 rich tuperssuatsiaite: a palygorskite-related mineral. American Mineralogist, 87, 1458–1463.
481 Chervonnyi, A.D., Chukanov, N.V., and Chervonnaya, N.A. (2010) Synthetic calcium
482 aluminosilicate monolith: III. The nature of binder and high-temperature behavior. Russian
483 Journal of Inorganic Chemistry, 55. 1521–1528.
484 Chukanov, N.V. (2014) Infrared Spectra of Mineral Species: Extended Library. Springer-Verlag,
485 Dordrecht, 1716 pp.
486 Chukanov, N.V. and Chervonnyi, A.D. (2016) Infrared Spectroscopy of Minerals and Related
487 Compounds. Springer Verlag, Cham, 1109 pp.
488 Chukanov, N.V., Britvin, S.N., Blass, G., Belakovskiy, D.I., and Van, K.V. (2012) Windhoekite,
489 $Ca_2Fe^{3+}_{3-x}(Si_8O_{20})(OH)_4 \cdot 10H_2O$, a new palygorskite-group mineral from the Aris phonolite,
490 Namibia. European Journal of Mineralogy, 24, 171–179.
491 Churakov, S.V. (2009) Structural position of H_2O molecules and hydrogen bonding in anomalous
492 11Å tobermorite. American Mineralogist, 94, 156–165.
493 Claringbull, G.F. and Hey, M.H. (1952) A reexamination of tobermorite. Mineralogical Magazine,
494 29, 960–962.
495 Dornberger-Schiff, K. (1956) On the order-disorder (OD-structures). Acta Crystallographica, 9, 593.
496 Dornberger-Schiff, K. (1964) Grundzüge einer Theorie von OD-Strukturen aus Schichten.
497 Abhandlungen der Deutschen Akademie der Wissenschaften zu Berlin. Klasse für Chemie,
498 Geologie und Biologie, 3, 1–107.
499 Dornberger-Schiff, K. (1966) Lehrgang über OD-Strukturen, Akademie-Verlag, Berlin, 135 pp.

Dornberger-Schiff, K. and Fichtner, K. (1972) On the symmetry of OD-structures consisting of equivalent layers. Kristall und Technik, 7**,** 1035–1056.

El-Didamony, H., Khalil, K.A., and El-Attat, M.S. (2000) Physicochemical characteristics of fired clay-limestone mixtures. Cement and Concrete Research, 30, 7–11.

Erokhin, Yu.V. (2017) Bazhenovskoe Deposit (Central Urals, Russia): Mineralogy of Rodingites. Mineralogical Almanac, 22(3), 1–136.

Ferraris, G. and Gula, A. (2005) Polysomatic aspects in microporous minerals – heterophyllosilicates, palysepioles and rhodesite-related structures. Reviews in Mineralogy and Geochemistry. Micro- and Mesoporous Mineral Phases, 57, 69–104.

Ferraris, G., Makovicky, E. and Merlino, S. (2008) Crystallography of Modular Materials. Oxford, IUCr/Oxford University Press.

Gagné, O.C. and Hawthorne, F.C. (2015) Comprehensive derivation of bond-valence parameters for ion pairs involving oxygen. Acta Crystallographica, B71, 562–578.

Hamid, S.A. (1981) The crystal structure of the 11Å natural tobermorite $Ca_{2.25}[Si_3O_{7.5}(OH)_{1.5}]\cdot 1H_2O$. Zeitschrift für Kristallographie, 154, 189–198.

Heddle, M.F. (1880) Preliminary notice of substances which may prove to be new minerals. Mineralogical Magazine, 4, 117–123.

Henmi, C. and Kusachi, I. (1992) Clinotobermorite, $Ca_5Si_6(O,OH)_{18}\cdot 5H_2O$, a new mineral from Fuka, Okayama Prefecture, Japan. Mineralogical Magazine, 56, 353–358.

Hoffmann, C. and Armbruster, T. (1997) Clinotobermorite, $Ca_5[Si_3O_8(OH)]_2\cdot 4H_2O$ – $Ca_5[Si_6O_{17}]\cdot 5H_2O$, a natural C-S-H(I) type cement mineral: determination of the substructure. Zeitschrift für Kristallographie, 212, 864–873.

Kudoh, Y. and Takéuchi, Y. (1979) Polytypism in xonotlite: (I) Structure of an A-1 polytype, locality: Heguri, Chiba Prefecture, Japan. Mineralogical Journal (Japan), 9, 349–373.

524 Libowitzky, E. (1999) Correlation of O–H stretching frequencies and O–H···O hydrogen bond
525 lengths in minerals. Monatshefte für Chemie, 130, 1047–1059.
526 Ma, Z., Shi, N., Mou, G., and Liao, L. (1999) Crystal structure refinement of suolunite and its
527 significance to the cement techniques. Chinese Science Bulletin, 44, 2125–2130.
528 Mamedov, Kh.S and Belov, N.V. (1958) On the crystal structure of tobermorite (tobermorites).
529 Doklady Akademii Nauk SSSR, 123(1), 163–165 (in Russian).
530 Mandarino, J.A. (1981) The Gladstone-Dale relationship, Part IV. The compatibility concept and its
531 application. The Canadian Mineralogist, 19, 441–450.
532 McConnell, J.D.C. (1954) The hydrated calcium silicates riversideite, tobermorite, and plombierite.
533 Mineralogical Magazine, 30, 293–305.
534 Megaw, H.D. and Kelsey, C.H. (1956) Crystal structure of tobermorite. Nature, 177, 390–391.
535 Merlino, S. and Bonaccorsi, E. (2008) Double wollastonite chains: topological/conformational
536 varieties, polytypic forms, isotypic compounds. Zeitschrift für Kristallographie, 223, 85–97.
537 Merlino, S., Bonaccorsi, E., and Armbruster, T. (1999) Tobermorites: Their real structure and order-
538 disorder (OD) character. American Mineralogist, 84, 1613–1621.
539 Merlino, S., Bonaccorsi, E., and Armbruster, T. (2000) The real structures of clinotobermorite and
540 tobermorite 9 Å: OD character, polytypes, and structural relationships. European Journal of
541 Mineralogy, 12, 411–429.
542 Merlino, S., Bonaccorsi, E., and Armbruster, T. (2001) The real structure of tobermorite 11Å:
543 normal and anomalous forms, OD character and polytypic modifications. European Journal of
544 Mineralogy, 13, 577–590.
545 Organova, N.I., Koporulina, E.V., Ivanova, A.G., Trubkin, N.V. Zadov, A.E., Khomyakov, A.P.,
546 Marcille, I.M., Chukanov, N.V., and Shmakov, A.N. (2002) Structure model of Al,K-
547 substituted tobermorite and structural changes upon heating. Crystallography Reports, 47(6),
548 950–956.

549 Pekov, I.V., Zubkova, N.V., Chukanov, N.V., Yapaskurt, V.O., Britvin, S.N., Kasatkin, A.V., and
550 Pushcharovsky D.Y. (2019) Oyelite: new mineralogical data, crystal structure model and
551 refined formula $Ca_5BSi_4O_{13}(OH)_3 \cdot 4H_2O$. European Journal of Mineralogy, 31, 595–608.
552 Richardson, L.G. (2008) The calcium silicate hydrates. Cement and Concrete Research, 38, 137–
553 158.
554 Rigaku Oxford Diffraction (2018) CrysAlisPro Software System, v. 1.171.39.46, Rigaku
555 Corporation, Oxford, UK.
556 Saburi, S., Kawahara, A., Henmi, C., Kusachi, I., and Kihara, K. (1977) The refinement of the
557 crystal structure of cuspidine. Mineralogical Journal, 8(5), 286–298.
558 Sakiyama, M., Maeshima, T., and Mitsuda, T. (2000) Synthesis and crystal chemistry of Al-
559 substituted 11 Å tobermorite. Journal of the Society of Inorganic Materials of Japan, 7, 413–
560 419.
561 Sheldrick, G.M. (2015) Crystal structure refinement with SHELXL. Acta Crystallographica, C71, 3–
562 8.
563 Spek, A.L. (2003) Single-crystal structure validation with the program PLATON. Journal of
564 Applied Crystallography, 36, 7–13.
565 Taylor, H.F.W. (1953) Hydrated calcium silicates. Part V. The water content of calcium silicate
566 hydrate (I). Journal of the Chemical Society, 12, 163–171.
567 Taylor, H.F.W. (1964) The calcium silicate hydrates. Chemistry of Cements. Vol. 1. (ed. H.F.W.
568 Taylor). Academic Press, London, 167–232.
569 Taylor, H.F.W. (1971) The crystal structure of kilchoanite. Mineralogical Magazine, 38, 26–31.
570 Tsuji, M., Komarneni, S., and Malla, P. (1991) Substituted tobermorites: ^{27}Al and ^{29}Si MASNMR,
571 cation exchange, and water sorption studies. Journal of American Ceramic Society, 74, 274–
572 279.

573 Zadov, A.E., Chukanov, N.V., Organova, N.I., Belakovskiy, D.I., Fedorov, A.V., Kartashov, P.M.,
574 Kuz'mina O.V., Litsarev, M.A., Mokhov, A.V., Loskutov, A.B., and Fin'ko, V.I. (1995) New
575 finds and studies of tobermorite-group minerals. Zapiski Vserossiiskogo Mineralogicheskogo
576 Obshchestva, 124(2), 36–54 (in Russian).
577 Zadov, A.E., Chukanov, N.V., Organova, N.I., Kuz'mina O.V., Belakovskiy, D.I., Nechay, V.G.,
578 Sokolovskiy, F.S., and Kuznetsova, O.Yu. (2000) Comparative study of rosenhahnite from
579 California and Urals. Refinement of formula. Zapiski Vserossiiskogo Mineralogicheskogo
580 Obshchestva, 129(2), 85–96 (in Russian).
581 Zadov, A.E., Chukanov, N.V., Organova, N.I., Kuz'mina O.V., Belakovskiy, D.I., Litsarev, M.A.,
582 Nechay, V.G., and Sokolovskiy, F.S. (2001) Hydration, dehydration and thermal
583 transformations of tobermorite-group minerals. Zapiski Vserossiiskogo Mineralogicheskogo
584 Obshchestva, 130(2), 26–40 (in Russian).

585 Zadov, A.E., Grabezhev, A.I., Pertsev, N.N., Chukanov, N.V., and Pribavkin, S.V. (2006)

586 Tobermorite-plombierite metasomatites of the Gumeshevsk skarn-porphyry copper deposit, middle

587 Urals. Doklady Earth Sciences, 407(2), 495–497.

588 **Figure captions**

589

590 **Figure 1.** Two topological types of the complex Ca-*T*-O module, a fundamental building unit in the
591 crystal structures of tobermorite-supergroup minerals: (a) complex module of type A in
592 paratobermorite and (b) complex module of type B in tobermorite (drawn after Merlino et al. 2001).

593

594 **Figure 2.** The crystal structure of paratobermorite (a) and tobermorite (drawn after Merlino et al.
595 2001) (b). The unit cells are outlined.

596

597 **Figure 3.** OD Layer in tobermorite 11Å (taken from Merlino et al., 2001). The λ operations are
598 indicated.

599

600 **Figure 4.** Paratobermorite crystal.

601

602 **Figure 5.** Crystals (a, b) and open-work crystal cluster of paratobermorite. SEM images: a – BSE
603 mode, b and c – SE mode.

604

605 **Figure 6.** Paratobermorite aggregates: a – open-work aggregates on almost colourless grossular
606 crystal crust with small milky-white spherulites of pectolite-1*A* (photo: I.V. Pekov & A.V.
607 Kasatkin); b – radial cluster of prismatic crystals (length of the largest, divergent crystal is 8 mm) on
608 prehnite spherulitic crust, which covers a wall of cavity in grossular rodingite (photo: N.N.
609 Koshlyakova). FOV width: a – 7.5 mm, b – 1.5 cm.

610

611 **Figure 7.** Powder infrared absorption spectra of (*a*) paratobermorite and (*b*) Al-free tobermorite-2*M*
612 with the empirical formula $Ca_{4.68}Si_6O_{16.36}(OH)_{0.64}\cdot nH_2O$ ($n \sim 5$) from the Pervomaiskiy quarry, Mt.
613 Bol'shoy Kermen, Bakhchisaray district, Crimea Peninsula.
614
615 **Figure 8.** Tetrahedral motifs in the structures of 2*M* polytypes of 'tobermorites 11 Å':
616 paratobermorite (a; for legend see Fig. 2; *T*3- and *T*4-centred tetrahedra are filled alternatively and
617 *T*4 tetrahedra are not shown here for better clarity), tobermorite (b; drawn after Merlino et al. 2001)
618 and clinotobermorite (c; drawn after Merlino et al. 2000). The unit cells are outlined.
619

This is the peer-reviewed, final accepted version for American Mineralogist, published by the Mineralogical Society of America.
The published version is subject to change. Cite as Authors (Year) Title. American Mineralogist, in press.
DOI: https://doi.org/10.2138/am-2022-8284. http://www.minsocam.org/

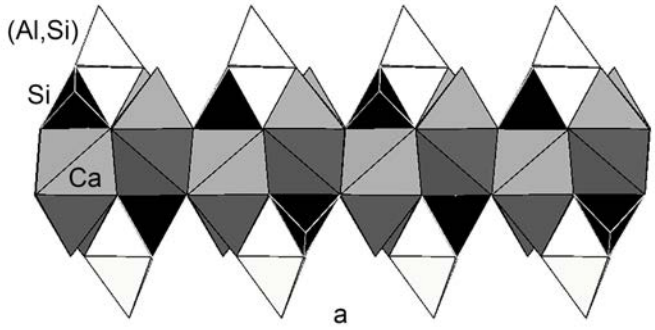

Figure 1a

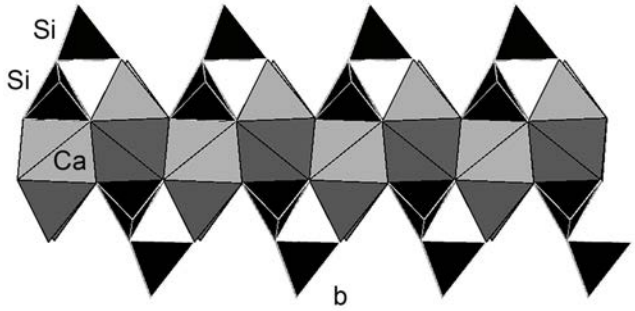

Figure 1b

This is the peer-reviewed, final accepted version for American Mineralogist, published by the Mineralogical Society of America.
The published version is subject to change. Cite as Authors (Year) Title. American Mineralogist, in press.
DOI: https://doi.org/10.2138/am-2022-8284. http://www.minsocam.org/

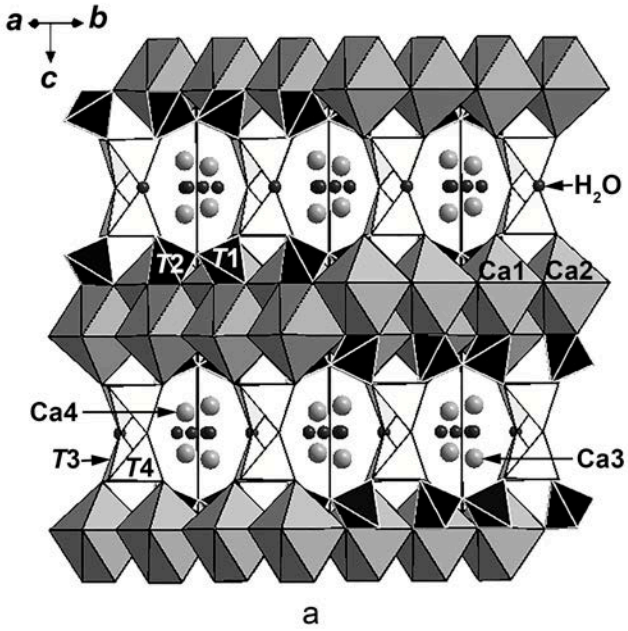

Figure 2a

627

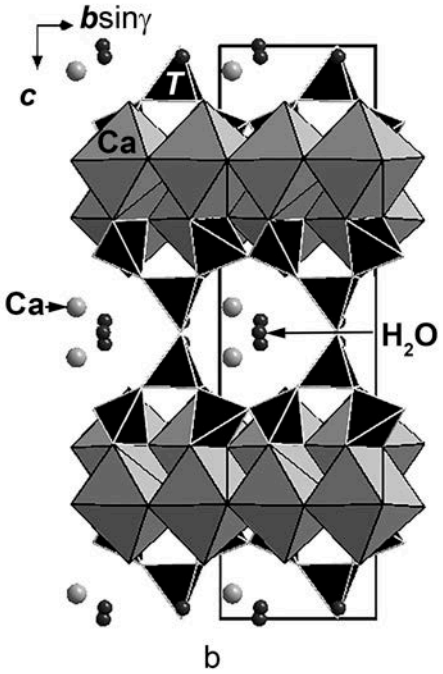

Figure 2b

628

This is the peer-reviewed, final accepted version for American Mineralogist, published by the Mineralogical Society of America.
The published version is subject to change. Cite as Authors (Year) Title. American Mineralogist, in press.
DOI: https://doi.org/10.2138/am-2022-8284. http://www.minsocam.org/

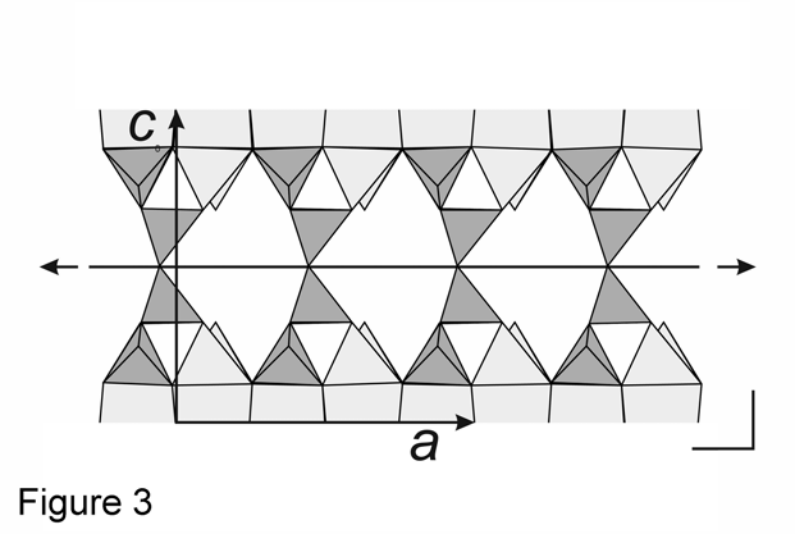

Figure 3

629

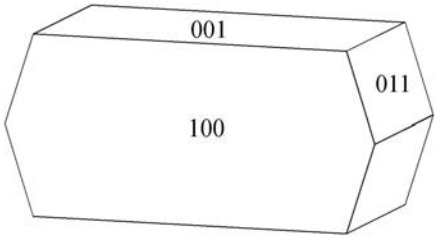

Figure 4

630

631

This is the peer-reviewed, final accepted version for American Mineralogist, published by the Mineralogical Society of America.
The published version is subject to change. Cite as Authors (Year) Title. American Mineralogist, in press.
DOI: https://doi.org/10.2138/am-2022-8284. http://www.minsocam.org/

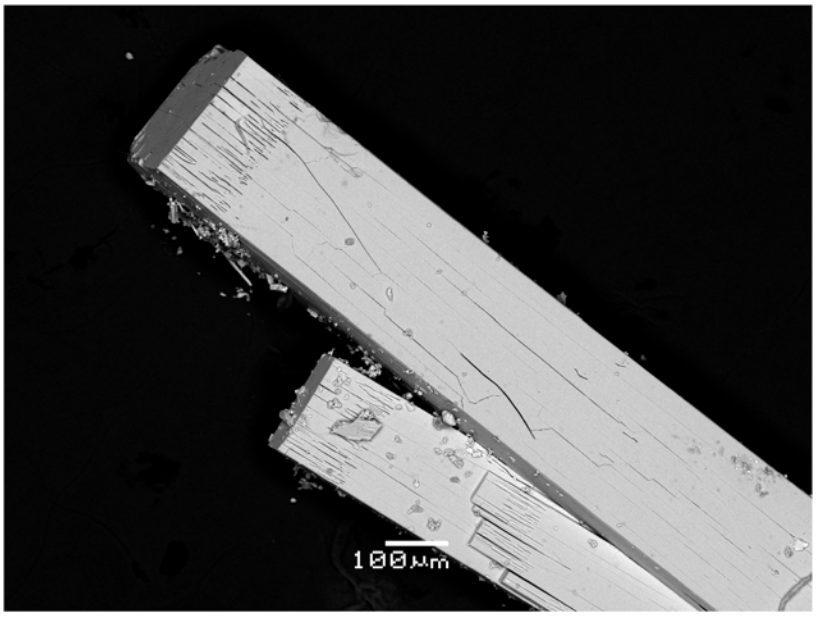

a

632 Figure 5a

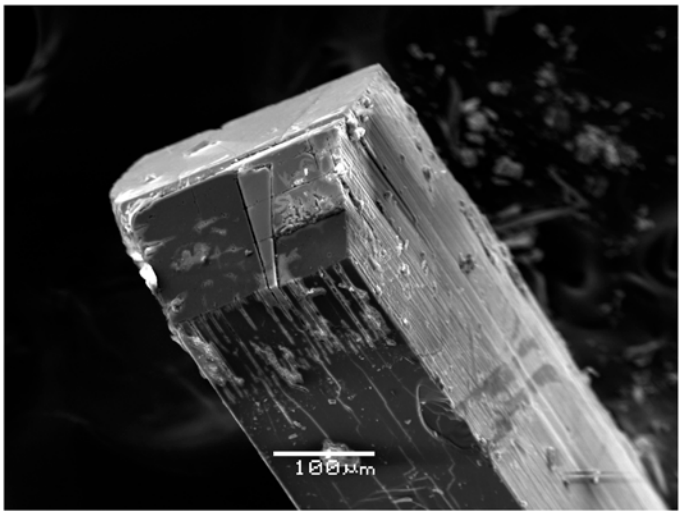

b

633 Figure 5b
634
635
636

This is the peer-reviewed, final accepted version for American Mineralogist, published by the Mineralogical Society of America.
The published version is subject to change. Cite as Authors (Year) Title. American Mineralogist, in press.
DOI: https://doi.org/10.2138/am-2022-8284. http://www.minsocam.org/

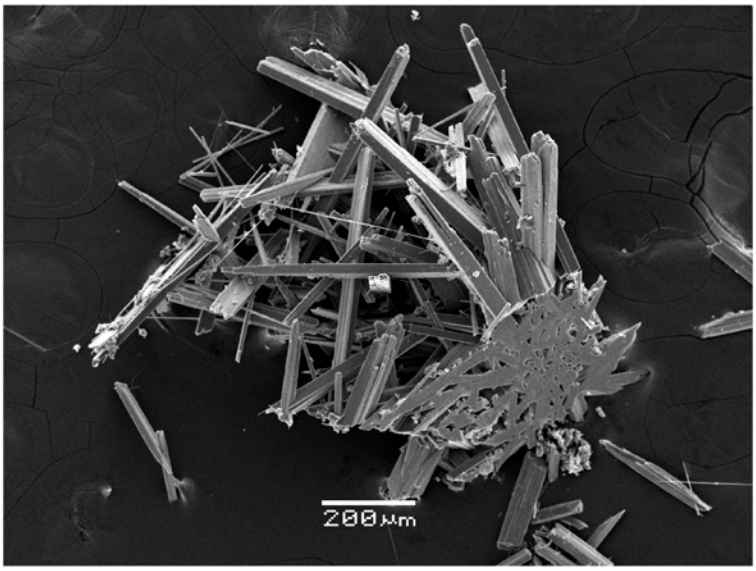

c

Figure 5c

This is the peer-reviewed, final accepted version for American Mineralogist, published by the Mineralogical Society of America.
The published version is subject to change. Cite as Authors (Year) Title. American Mineralogist, in press.
DOI: https://doi.org/10.2138/am-2022-8284. http://www.minsocam.org/

641

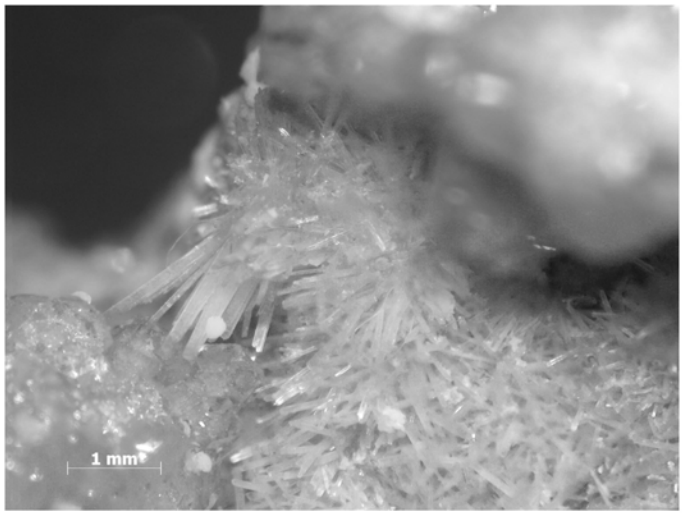

a

642 Figure 6a

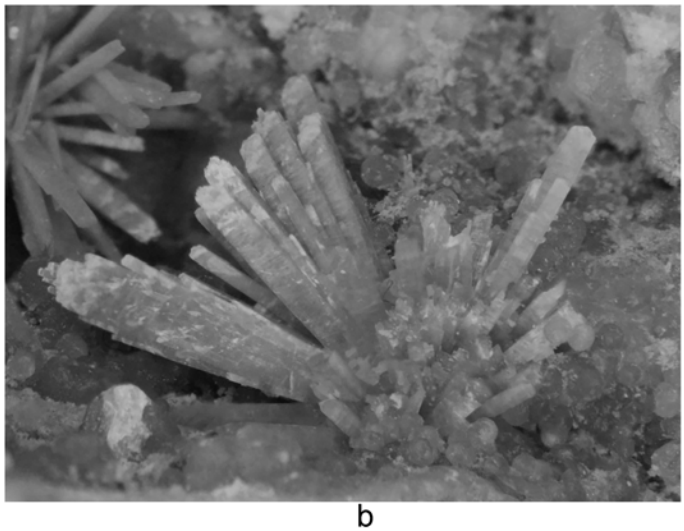

b

643 Figure 6b

644

645

646

This is the peer-reviewed, final accepted version for American Mineralogist, published by the Mineralogical Society of America.
The published version is subject to change. Cite as Authors (Year) Title. American Mineralogist, in press.
DOI: https://doi.org/10.2138/am-2022-8284. http://www.minsocam.org/

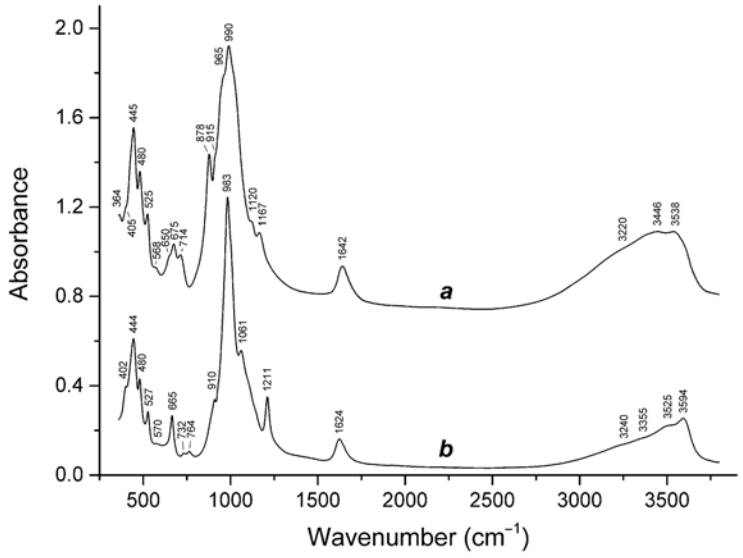

Figure 7

647

648

649

This is the peer-reviewed, final accepted version for American Mineralogist, published by the Mineralogical Society of America.
The published version is subject to change. Cite as Authors (Year) Title. American Mineralogist, in press.
DOI: https://doi.org/10.2138/am-2022-8284. http://www.minsocam.org/

650

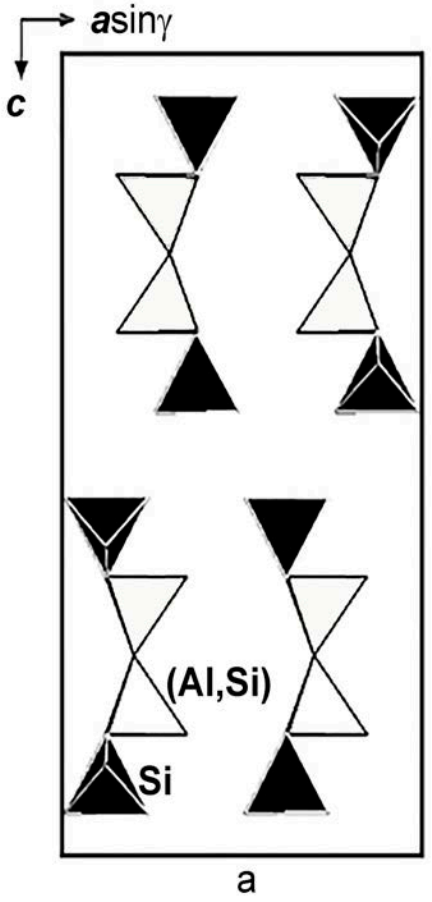

Figure 8a

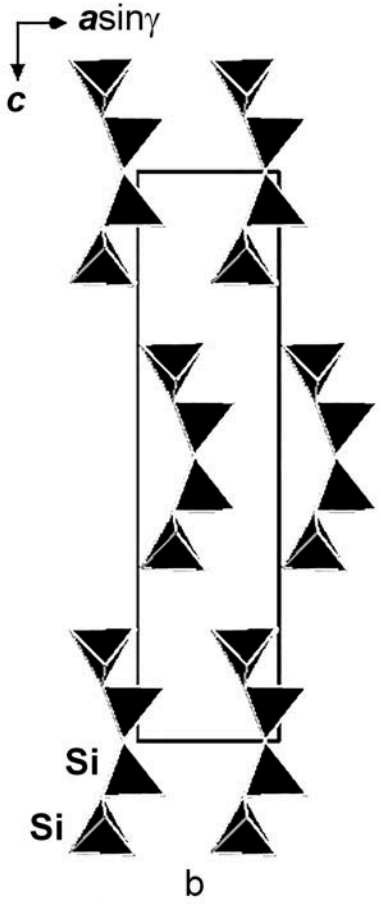

Figure 8b

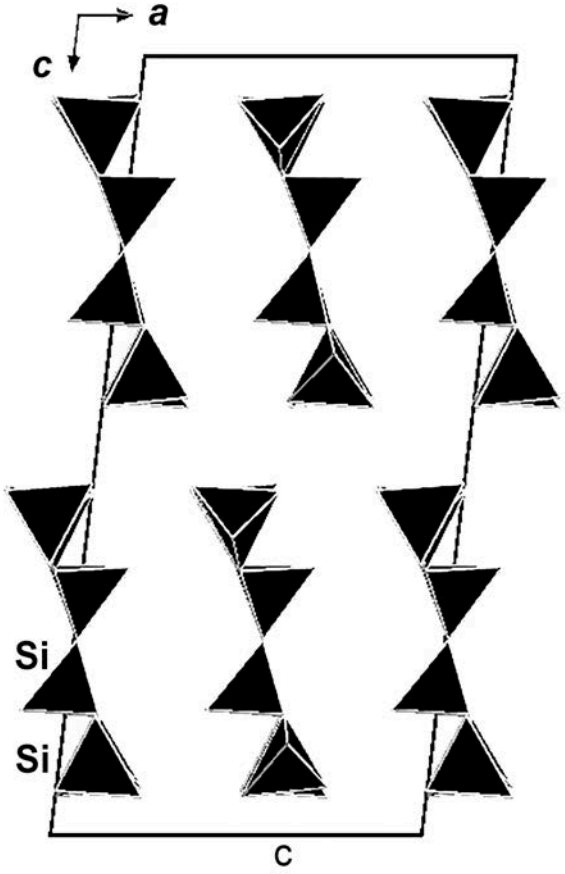

Figure 8c

This is the peer-reviewed, final accepted version for American Mineralogist, published by the Mineralogical Society of America.
The published version is subject to change. Cite as Authors (Year) Title. American Mineralogist, in press.
DOI: https://doi.org/10.2138/am-2022-8284. http://www.minsocam.org/

Tables

Table 1. Crystal data of tobermorite-supergroup minerals belonging to 'tobermorites 11 Å': tobermorite, clinotobermorite, kenotobermorite and paratobermorite (all polytypes known in nature are included)

Mineral	Paratobermorite	Tobermorite	Kenotobermorite		Clinotobermorite	
Simplified formula	$Ca_5AlSi_5O_{16}(OH)\cdot 5H_2O$	$Ca_5Si_6O_{17}\cdot 5H_2O$	$Ca_4Si_6O_{15}(OH)_2\cdot 5H_2O$		$Ca_5Si_6O_{17}\cdot 5H_2O$	
Ideal (structural) formula*	$[Ca_4(Al_{0.5}Si_{0.5})_2Si_4O_{16}(OH)\cdot 2H_2O]\cdot(Ca\cdot 3H_2O)$	$[Ca_4Si_6O_{17}\cdot 2H_2O]\cdot(Ca\cdot 3H_2O)$	$[Ca_4Si_6O_{15}(OH)_2\cdot 2H_2O]\cdot(3H_2O)$		$[Ca_4Si_6O_{17}\cdot 2H_2O]\cdot(Ca\cdot 3H_2O)$	
Polytype	2*M*	2*M*	2*M*	4*O*	2*M*	1*A*
Crystal system Space group	Monoclinic $C112_1/m$	Monoclinic $B11m$	Monoclinic $B11m$	Orthorhombic $F2dd$	Monoclinic Cc	Triclinic $C1$
a, Å	11.2220 (4)	6.732	6.735	11.265	11.276	11.274
b, Å	7.3777 (2)	7.369	7.385	7.385	7.343	7.344
c, Å	22.9425 (8)	22.680	22.487	44.970	22.642	11.468
α, º	90	90	90	90	90	99.18
β, º	90	90	90	90	97.28	97.19
γ, º	89.990 (3)	123.18	123.25	90	90	90.02
V, Å^3	1899.46 (10)	942	935	3742	1860	930
Z	4	2	2	8	4	2
Source	This work	Merlino et al. 2001; Biagioni et al. 2015	Merlino et al. 1999, 2001; Biagioni et al. 2015		Merlino et al. 1999, 2000; Biagioni et al. 2015	

Unit cells of all listed minerals are given in the same setting corresponding to the orientation of layers of Ca-polyhedra in the *ab* plane.
Plombiérite ('tobermorite 14 Å') and insufficiently studied riversideite ('tobermorite 9 Å') are not included.
* Written in accordance with the IMA-accepted nomenclature of tobermorite-supergroup minerals (Biagioni et al. 2015).

This is the peer-reviewed, final accepted version for American Mineralogist, published by the Mineralogical Society of America.
The published version is subject to change. Cite as Authors (Year) Title. American Mineralogist, in press.
DOI: https://doi.org/10.2138/am-2022-8284. http://www.minsocam.org/

659 **Table 2**. Chemical composition (wt.%) of paratobermorite

Constituent	Mean*	Range	Stand. Dev. (σ)	Probe standard
Na_2O	0.40	0.29 – 0.47	0.08	NaCl
K_2O	0.28	0.23 – 0.33	0.04	microcline
CaO	36.60	36.26 – 36.82	0.26	plagioclase
MnO	0.04	0.00 – 0.11	0.04	$MnTiO_3$
BaO	0.07	0.00 – 0.14	0.06	BaF_2
Al_2O_3	6.46	6.30 – 6.72	0.19	plagioclase
SiO_2	42.32	42.03 – 42.71	0.32	diopside
H_2O	14.10	13.83 – 14.37		
Total	100.27			

660 * Averaged for four spot analyses. Contents of other elements with atomic numbers higher than that
661 of carbon are below detection limits.

662

663

This is the peer-reviewed, final accepted version for American Mineralogist, published by the Mineralogical Society of America.
The published version is subject to change. Cite as Authors (Year) Title. American Mineralogist, in press.
DOI: https://doi.org/10.2138/am-2022-8284. http://www.minsocam.org/

664 **Table 3**. Powder X-ray diffraction data (*d* in Å) of paratobermorite

I_{obs}	d_{obs}	I_{calc}*	d_{calc}**	*h k l*
100	**11.52**	100	11.471	002
5	6.17	1	6.165	110
5	5.97	1, 1	5.954, 5.954	111, -111
3	5.76	3	5.736	004
24	**5.46**	17, 1, 2	5.450, 5.431, 5.431	201, 112, -112
2	4.808	3	4.800	113
3	3.836	2	3.824	006
4	3.650	2, 3	3.681, 3.642	115, 021
17	**3.562**	13	3.552	205
11	3.329	1, 5, 1	3.337, 3.323, 3.302	310, 023, 311
4	3.259	6	3.249	-116
3	3.211	1	3.204	312
51	**3.088**	18, 16, 2	3.083, 3.083, 3.058	220, -220, -313
50	**2.982**	20, 14	2.977, 2.977	222, -222
10	2.878	3, 1, 1, 6	2.894, 2.884, 2.875, 2.868	117, 314, 025, 008
20	**2.838**	18	2.830	207
11	2.813	9	2.806	400
6	2.729	3, 1, 1	2.725, 2.715, 2.715	402, 224, -224
9	2.526	6	2.520	404
7	2.456	6	2.450	027
9	2.328	9	2.321	209
7	2.302	7	2.294	0.0.10
10	2.148	3, 4	2.144, 2.144	423, -423
7	2.104	2, 1, 3	2.100, 2.100, 2.097	228, -228, 029
14	**2.013**	7, 6	2.008, 2.008	425, -425
22	**1.848**	5, 9, 11, 2, 2	1.846, 1.846, 1.844, 1.840, 1.840	427, -427, 040, 2.2.10, -2.2.10
3	1.823	2	1.821	042
2	1.736	2	1.732	605
8	1.685	2, 4, 4	1.683, 1.680, 1.680	2.0.13, 429, -429
8	1.672	4, 4	1.668, 1.668	620, -620
3	1.641	1, 1	1.639, 1.637	0.0.14, -245
7	1.629	6	1.624	607
1	1.603	1	1.600	339
2	1.555	2	1.551	048
3	1.549	2, 2	1.545, 1.545	247, -247
1	1.530	1, 1	1.531, 1.528	-3.3.10, 442
1	1.480	1	1.476	2.0.15
3	1.447	1, 2	1.444, 1.444	249, -249
2	1.406	3	1.403	800
2	1.395	2	1.392	802

665 * For the calculated pattern, only reflections with intensities ≥1 are given; ** for the unit-cell
666 parameters calculated from single-crystal data; the strongest reflections are marked in bold.

667
668

This is the peer-reviewed, final accepted version for American Mineralogist, published by the Mineralogical Society of America.
The published version is subject to change. Cite as Authors (Year) Title. American Mineralogist, in press.
DOI: https://doi.org/10.2138/am-2022-8284. http://www.minsocam.org/

669
670
671
672
673
674 **Table 4**. Selected interatomic distances (Å) in the structure of paratobermorite
675

Ca1 – O1	2.315(7)	Ca3 – Ow3	2.05(5)
– O2	2.360(7)	– O7	2.126(12)
– O3	2.405(8)	– Ow2	2.30(5)
– O4	2.423(8)	– Ow4	2.32(7)
– O1	2.505(6)	– O8	2.328(11)
– O9	2.545(11)	– O6	2.720(14)
– O2	2.547(6)	– O5	2.775(14)
Ca2 – O4	2.340(8)	Ca4 – Ow5	2.04(6)
– O3	2.360(8)	– O9	2.24(2)
– O2	2.451(7)	– Ow1	2.25(3)
– O8	2.461(8)	– O7	2.49(2)
– O1	2.477(7)	– O6	2.85(2)
– O4	2.550(6)	– O5	2.98(2)
– O3	2.612(7)		
*T*1 – O3	1.603(6)	*T*3 – O*T*3	1.634(3)
– O4	1.612(6)	– O6	1.698(9)
– O5	1.615(8)	– O5	1.721(9)
– O7	1.639(8)	– O8	1.728(9)
*T*2 – O2	1.565(6)	*T*4 – O6	1.694(12)
– O1	1.603(6)	– O*T*4	1.705(9)
– O6	1.645(7)	– O5	1.704(12)
– O7	1.649(8)	– O9	1.806(12)

676
677

This is the peer-reviewed, final accepted version for American Mineralogist, published by the Mineralogical Society of America.
The published version is subject to change. Cite as Authors (Year) Title. American Mineralogist, in press.
DOI: https://doi.org/10.2138/am-2022-8284. http://www.minsocam.org/

678 **Table 5**. Bond-valence calculations for paratobermorite
679

Site	Ca1	Ca2	*T*1	*T*2	*T*3 = $Al_{0.35}Si_{0.35}$	*T*4 = $Al_{0.15}Si_{0.15}$	Ca3 = $Ca_{0.25}$	Ca4 = $Ca_{0.125}$	Σ
O1 = O	0.37 0.23	0.25		1.06					1.91
O2 = O	0.33 0.21	0.26		1.16					1.96
O3 = O	0.30	0.33 0.18	1.06						1.87
O4 = O	0.28	0.35 0.21	1.03						1.87
O5 = O			1.02		0.55	0.25	0.03	0.01	1.86
O6 = O				0.95	0.60	0.26	0.03	0.01	1.85
O7 = O			0.96	0.94			0.14	0.03	2.07
O8 = $O_{0.25}(OH)_{0.45}(H_2O)_{0.3}$		0.26			0.55		0.09		0.90
O9 = $(OH)_{0.3}(H_2O)_{0.7}$	0.21					0.19		0.06	0.46
O*T*3 = $O_{0.70}$					$0.69^{x2\rightarrow}$				1.38
O*T*4 = $O_{0.30}$						$0.25^{x2\rightarrow}$			0.50
Ow1 = $H_2O_{0.50}$								0.05 x2→	0.10
Ow2 = $H_2O_{0.50}$							0.10 x2→		0.20
Ow3 = $H_2O_{0.50}$							0.18 x2→		0.36
Ow4 = $H_2O_{0.50}$							0.09 x2→		0.18
Ow5 = $H_2O_{0.50}$								0.09 x2→	0.18
Σ	1.93	1.84	4.07	4.11	2.39	0.95	0.66	0.25	

680 Bond-valence parameters were taken from Gagné and Hawthorne (2015).